Energy

Volume 165, Part A, 15 December 2018, Pages 512-521

Reverse Electrodialysis for energy production from natural River Water and Seawater[1]

Ahmet H. Avci[1], Ramato A. Tufa[2], Enrica Fontananova[3], Gianluca Di Profio[3], Efrem Curcio[1,3]*

[1] Department of Environmental and Chemical Engineering, University of Calabria DIATIC-UNICAL, Via P. Bucci CUBO 45A, 87036 Rende (CS) Italy

[2] Department of Inorganic Technology, University of Chemistry and Technology Prague, Technická 5, 166 28 Prague 6, Czech Republic

[3] Institute on Membrane Technology, National Research Council of Italy ITM-CNR, Via P. Bucci CUBO 17C, 87036 Rende (CS) Italy

Abstract

The effectiveness of Salinity Gradient Power - Reverse Electrodialysis (SGP-RE) in real practice is still not clearly defined due to the lack of specific studies in literature, being investigations in large part limited to on pure NaCl solutions or aqueous mixtures of two salts. In this work, we experimentally assessed the impact of natural feed streams (collected from Licetto river and Tyrrenian sea in Amantea - Italy) in terms of Open Circuit Voltage (OCV) and power density (P_d) measured on lab-scale SGP-RE stack prototype; results have been compared to those obtained when using NaCl solutions having equivalent ionic strength. Highest OCV (3.68 V and 4.09 V) and P_d values (0.46 and 1.41 $W \cdot m^{-2}$) were observed at temperature of 60°C for real and synthetic feeds, respectively.

The extent of electrical resistances (ion exchange membrane/electrical double layer/diffusion boundary layer) was elucidated by electrochemical impedance spectroscopy (EIS); in particular, a critical effect of real solution on cation exchange membrane (CEM) resistance was detected. In

[1] DOI: 10.1016/j.energy.2018.09.111

addition, ionic characterization of process effluents revealed the occurrence of uphill transport of multivalent ions Mg^{2+}, Ca^{2+} and SO_4^{2-}.

Keywords: *Reverse Electrodialysis; Salinity Gradient Power; natural feeds; Electrochemical Impedance Spectroscopy; Uphill transport*

* e.curcio@unical.it (corresponding author)

1. Introduction

According to US Energy Information Administration, world net electricity generation is expected to increase from 20 trillion to 40 trillion kWh in the coming 30 years; among all sources which presently fulfill the increasing demand of energy, renewable energy is the fastest-growing source of electric power with an annual 2.8% increase [1]. An emerging renewable energy source is Salinity Gradient Power (SGP), originally proposed for sea and river water mixing more than 60 years ago [2]. The total technical potential of SGP is estimated to be around 647 GW, which is 23% of the global electricity consumption [3]. Possible application areas of SGP techniques are estuaries where freshwater rivers run into seawater [4–7], high salinity wastewater (brine from desalination [8–11] or salt mining and saltworks [12–14]) and saltwater lakes [15,16].

There are two common technologies which harvest SGP by utilizing membrane-based processes: Reverse Electrodialysis (RE) – object of the present work - and Pressure Retarded Osmosis (PRO) [17]. In a typical SGP-RE system, cation exchange membranes (CEM) and anion exchange membranes (AEM) are piled up alternately between cathode and anode (Fig. 1). CEMs and AEMs are separated by spacers to allow the diluted and concentrated salt solutions flow through. Due to salinity gradient across the membranes, ions diffuse through the membranes from High Concentration Compartment (HCC) to Low Concentration Compartment (LCC): the ionic flux is

converted to electronic flux in the electrode compartments by reduction and oxidation reactions on the electrode surface [10].

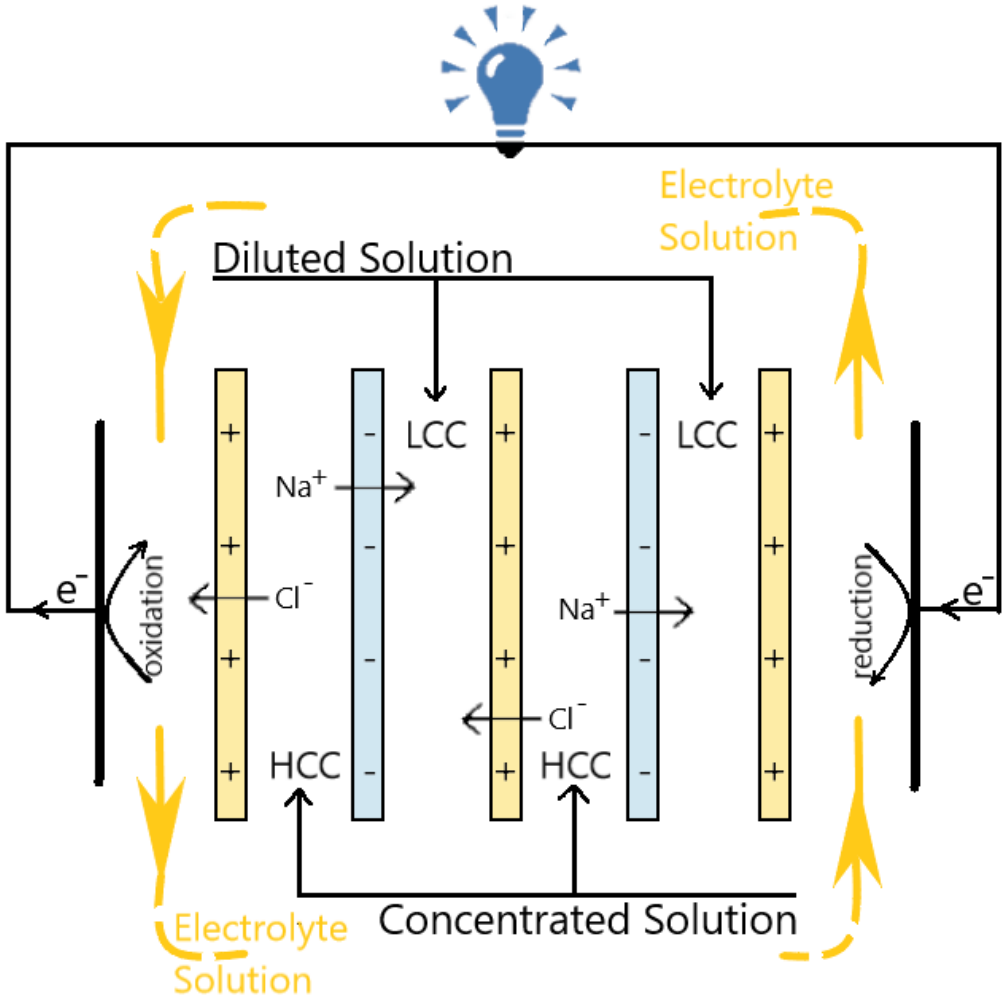

Figure 1. Conceptual scheme of a SGP-RE Unit

The most abundant natural salinity gradient sources are seawater and river water. Theoretically, the generated mixing energy of two solution with different concentration can be calculated by Gibbs free energy equation [6]:

$$\Delta G_{mix} = 2RT\left[V_D C_D \ln\frac{C_D}{C_M} + V_C C_C \ln\frac{C_C}{C_M}\right] \quad (1)$$

$$C_M = \frac{V_D C_D + V_C C_C}{V_D + V_C} \quad (2)$$

where ΔG_{mix} is the Gibbs free energy of mixing, V_D is volume of diluted solution with concentration C_D, V_C is volume of concentrated solution with concentration C_C, C_M is the concentration of mixed solution, R is the gas constant (R=8.31432 $Jmol^{-1}K^{-1}$) and T is the temperature (K). Eq. 1 assumes entropy change in the water and activity of the solutions having negligible effect on final ΔG_{mix}.

In theory, complete mixing of 1 m^3 seawater (assumed as 30 kg $\cdot m^{-3}$ NaCl) and 1 m^3 river water (assumed as pure water) produces 1.7 MJ energy, that can be increased up to 6.1 MJ at 298 K when volumetric ratio of river water/seawater is 10 [6]. The numerous attempts made to investigate extractable energy of seawater and river water mixing resulted in gross power density between 0.20 - 2.2 $W \cdot m^{-2}$ depending on membrane design [18–21], spacer design [7,22–24], stack design [25,26] and process conditions (i.e. slight difference on concentration gradient, flow properties and temperature) [2,7,27,28]. One of the first measurements of power density was reported as 0.20 $W \cdot m^{-2}$ by Pattle (1954). In that study, maximum power was obtained for polyethylene mixed with crosslinked polystyrene resins membranes and 1 mm nonconductive thickness at 39ºC where 0.5 M NaCl solution and tap water were used as feed [2]. After IEM technology had improved, Veerman *et al.* (2009) performed synthetic seawater/river water RE experiments with six commercial membranes pairs; the highest measured power densities were 1.17 and 1.18 $W \cdot m^{-2}$ for Fumasep (FAD and FDK) and Selemion (AMV and CMV) membrane pairs, respectively, and a noteworthy thermodynamic efficiency (35%) was obtained [18]. Guler *et al.* (2013) prepared custom-made sulfonated polyetheretherketone CEM and polyepichlorohydrin AEM designed for RE; utilizing these membrane pairs resulted in 1.28 $W \cdot m^{-2}$ gross power density [20]. Hong *et al.* (2014) conducted RE experiments by pairing a custom-made composite CEM with ASV

(Selemion, Japan) AEM; under optimized electrochemical properties, a maximum power density of 1.3 $W \cdot m^{-2}$ was generated [21]. Vermaas *et al.* (2011) investigated the effect of intermembrane thickness and feed flow rate on the power density for synthetic seawater and river water: the highest recorded gross power density was 2.2 $W \cdot m^{-2}$ for 100 μm intermembrane thickness; moreover, possibility to reach 4 $W \cdot m^{-2}$ was predicted for 60 μm intermembrane thickness [7].

Aforementioned studies were only carried out with synthetic solutions mimicked by NaCl. When mimicking natural solutions, synthetic solutions are basically prepared ions of interest. However, a large spectra of mono- and multivalent ions together with some organic compounds are present in the natural feed solutions. Although previous studies carried out on artificial multi-ion saline solutions revealed a drastic effect of these compounds on the RE performance [10,29–32], investigations on real environment are so far scarcely present in literature [14] and those studies prevalently focus on fouling phenomenon and the characteristic performance of the RED stack under such conditions [33–35]. The key observation of Vermaas *et al.* for a RED stack operated with natural seawater and river water was a drastic decrease in power density (40 %) due to significant organic fouling and associated increase in pressure drop [33]. On the other hand, Pawlowski *et al.* also investigated RED stack fed with natural river water and seawater but with relatively thicker spacers (800 μm) [34,35]. The use of such thick channels circumvented stack clogging and increase in pressure drop which was about 6 times slower than the case of Vermaas *et al.* [33]. However, none of this studies were supported by the characterization of membranes under realistic natural solutions to describe the global changes in stack performance.

Decrease in Nernst potential, uphill transport, increasing IEM resistance were the most pronounced observations due to presence of multivalent ions. Vermaas *et al.* (2014) and Post *et al.* (2009) investigated effect of divalent ions on stack voltage and resistance for artificial solutions

mimicking seawater/river water pair: up to 50% reduction in power density was observed when Mg^{2+} and SO_4^{2-} divalent ions were present [31,32]. For more concentrated solutions and for higher content of multivalent ions, more severe impact has been observed on RED performance. Tufa *et al.* (2014) observed 64% decrease in power density when a lab scale RED stack, installed with Fujifilm-80045 and Fujifilm-80050, operated with artificial solutions 0.083 M NaCl + 0.017 M $MgCl_2$/3.25 M NaCl + 1.75 M $MgCl_2$ instead of 0.1 M NaCl/5 M NaCl [10]. Avci *et al.* (2016) carried out a parametric work on concentration of Mg^{2+} for 0.5 and 4 molal solutions; having 100% Mg^{2+} instead of Na^+ resulted in more than 50% decrease on OCV, three times higher stack resistance and 90% decrease in produced gross power density [29]. Another study dealt with multi-ion solutions revealed that ground water (2.67 M)/seawater (0.79 M) mixing suffered from presence of other ions than Na^+ and Cl^-; such as CO_3^{2-}, Ca^{2+}, Mg^{2+} [30]. The first RE pilot plant was operated with natural brackish water and almost saturated brine from saltworks and compared with artificial NaCl equivalent solutions by Tedesco *et al.* (2016): the RE unit was able to generate 40 W power with 125 cell pairs and almost 50 m^2 membrane area for real waters whereas artificial NaCl solutions resulted in 65 W [14].

In the present study, the performance of SGP-RE was evaluated in a real environment by testing natural river water and seawater feeds. System performance was evaluated in terms of Open Circuit Voltage (OCV) and power density (P_d) on a lab-scale SGP-RE stack prototype, and results compared to those obtained when using NaCl solutions with equivalent ionic strength. The extent of electrical resistances (ion exchange membrane/electrical double layer/diffusion boundary layer) was elucidated by electrochemical impedance spectroscopy (EIS). Occurrence of uphill transport due to the presence of multivalent ions (Mg^{2+}, Ca^{2+} and SO_4^{2-}) was investigated by ion chromatography.

2. Materials and Methods

2.1. Solutions

Feed solutions were collected from river Licetto and Tyrrenian Sea in Amantea (Italy) and fed into lab scale RED stack without any treatment. In order to determine the ionic composition of the saline feeds, solutions were microfiltered through 0.20 μm pore size polypropylene membranes (Microdyn®), characterized by Ion Chromatography (see 2.3), is reported in Table 1.

Artificial aqueous solutions mimicking river water and seawater (same ionic strength) were prepared by appropriate amounts of NaCl (Sigma Aldrich, Italy). Ionic strength I_m of river and seawater was calculated as:

$$I_m = \frac{1}{2}\sum m_i z_i^2 \qquad (3)$$

where m_i is molality of the i-th ion and z_i its charge.

For SGP-RE operation, the composition of aqueous electrolyte solution was: 0.3 M potassium hexacyanoferrate (II), 0.3 M potassium hexacyanoferrate (III) and 2.5 M sodium chloride (all purchased from Sigma-Aldrich, Italy). For the preparation of synthetic saline solutions and electrolyte solution, deionized water (PURELAB, Elga LabWaters, 0.055 $mS \cdot cm^{-1}$) was used.

Table 1. Ionic composition of natural river water and seawater and equivalent ionic strength.

	Concentration (ppm)									Ionic Strength (molal)
	Na^+	K^+	Mg^{2+}	Ca^{2+}	Cl^-	NO_2^-	Br^-	NO_3^-	SO_4^{2-}	
River water	23	4	28	152	16	0.5	-	2	78	0.012
Seawater	17941	671	2121	493	20975	-	117	63	2192	0.958

2.2. Reverse Electrodialysis setup

The SGP-RE lab-scale prototype provided by REDstack BV (The Netherlands) was used in the same arrangement as described previously [29]. SGP-RE stack was equipped with AEM-80045 and CEM-80050 Ion Exchange Membranes (IEMs) provided by Fujifilm Manufacturing Europe B.V. (The Netherlands). Relevant characteristic of the membranes are illustrated in Table 2.

Table 2. Properties of ion exchange membrane [36]

Membrane code	Thickness (µm)*	Ion exchange capacity (mmol/g membrane)	Density of fixed charge (mol/L)	Membrane areal resistance (Ωcm^2)**
Fuji-AEM-80045	129 ± 2	1.4 ± 0.1	3.8 ± 0.2	1.551 ± 0.001
Fuji-CEM-80050	114 ± 2	1.1 ± 0.1	2.4 ± 0.2	2.974 ± 0.001

*Conditions: NaCl 0.5 M, 20°C
**Conditions: NaCl 0.5 M, 20°C, 2.8 cm/s

SGP-RE tests were carried out at different temperature (10-60 °C) and flow rate (20-40 $L \cdot h^{-1}$), as detailed in Table 3. LCC and HCC solutions were fed to the stack at the same temperature and flowrate; flowrate of electrolyte solution was fixed to 30 $L \cdot h^{-1}$. Solutions were fed by Masterflex L/S digital peristaltic pumps (Cole-Palmer, US) and conditioned to desired temperature by a refrigerated/heated circulating bath (PolyScience, US) before entering the stack.

A high dissipation five-decade resistance box in the range of 0.1–1000 Ω (CROPICO, Bracken Hill, US) was used to load the SGP-RE system. Corresponding voltage drop and current were recorded after altering resistance box in the range of 60–0.1 Ω. DC voltage drop across the stack was measured by a 3½ digital multimeter with accuracy of 70.5% in the range of 200 mV to 200 V (Velleman, DVM760, Belgium), and the current flowing across the load resistors was measured by 6½ digit multimeter (Agilent, 34422A, Italy).

After fitting voltage (V) versus current (I) with a straight line, OCV and the total resistance of stack (R_{stack}) (Ω) were respectively calculated as intercept (I=0) and slope of the equation:

$$V(I) = E_{OCV} - R_{stack} I \quad (4)$$

The gross power density P_d follows a parabolic trendline in the form of:

$$P_d = \frac{E_{OCV}^2}{4 R_{stack} N_M} \quad (5)$$

in which P_d is the gross power density (in $W \cdot m^{-2}$), OCV is the open circuit voltage, i.e., the stack voltage measured at zero current (V), R_{stack} is the internal resistance of the stack ($\Omega \cdot m^2$) and N_M is the number of membranes contributing to the voltage. P_d reaches its maximum value when external resistance (load resistance) is equal to internal resistance (stack resistance) [7].

2.3. Ion Chromatography

"Ion Chromatography was employed to quantify the concentration of ions at the inlet and outlet of SGP-RE unit (Metrohm 861 Advanced Compact Ion Chromatograph) operated under conditions reported in Table 3, in open- circuit configuration and continuous feed flow. In order to reach the steady-state, samples were collected after one hour of operation. Samples were characterized at room temperature, at which ion chromatograph was calibrated. 3.2 mM Na_2CO_3 + 1 mM $NaHCO_3$ was used as eluent for anion column Metrosep A Supp 5 - 250/4.0, and 2 mM nitric acid + 0.25 mM oxalic acid was used as eluent for cation column Metrosep C4 – 250/4.0."

Ion Chromatography was employed to quantify the concentration of ions at the inlet and outlet of SGP-RE unit (Metrohm 861 Advanced Compact Ion Chromatograph) operated under open- circuit configuration and continuous feed flow. In order to reach the steady-state, samples were collected after one hour of operation. 3.2 mM Na_2CO_3 + 1 mM $NaHCO_3$ was used as eluent for anion column Metrosep A Supp 5 - 250/4.0, and 2 mM nitric acid + 0.25 mM oxalic acid was used as eluent for cation column Metrosep C4 – 250/4.0.

2.4. Electrochemical Impedance Spectroscopy

Electrochemical Impedance Spectroscopy (EIS) measurements were carried out using a potentiostat/galvanostat combined with a frequency response analyzer (Metrohm Autolab PGSTAT302N). A home-designed four electrodes impedance cell having 3.14 cm^2 active membrane area (Fig. 2) was employed. Electro-deposition method was applied to cover working and counter electrodes with a thin layer of AgCl. The sense and reference electrodes were Ag/AgCl electrodes (Gamry Instruments); the Haber–Luggin capillaries were filled with 3 M KCl.

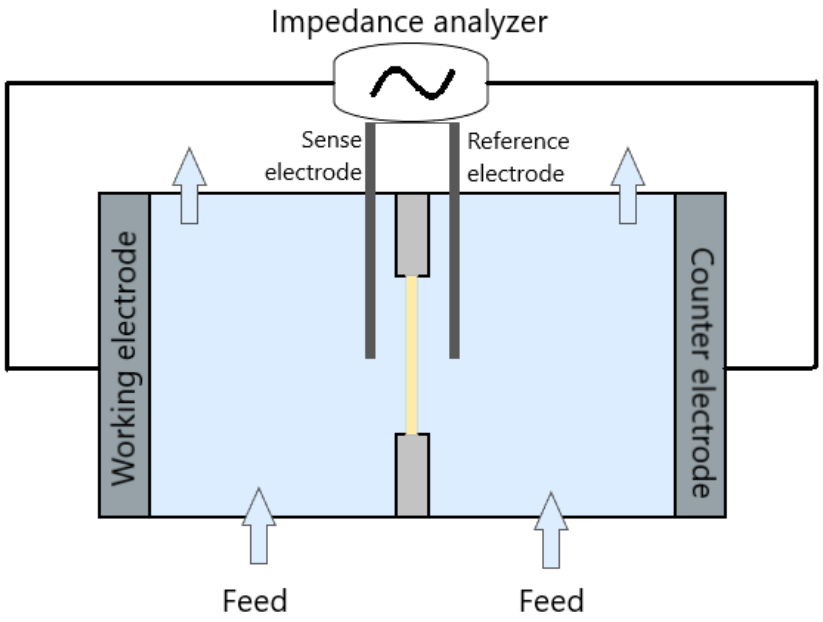

Figure 2. Scheme of four electrode confuguration Electrochemical Impedance Spectroscopy (EIS) cell.

AEM-80045 and CEM-80050 membranes were characterized by EIS for natural sea and river water at 25 °C. Before analysis, virgin membranes were conditioned for 24 h in test solutions, refreshed every 8 h to be sure no residual solutions were present.

Fig. 3 summarizes EIS procedure adopted in this study. AC current in the frequency range of 1000–0.01 Hz with signal amplitude of 10 mV was generated through the cell and response was recorded. Collected data were fitted by the equivalent circuit model shown in Fig. 3c by Nova 1.9.16 by Metrohm Autolab B.V (The Netherlands). Specifically, diffusion boundary layer was represented by a resistor and a constant phase element in parallel, while electric double layer was represented by a parallel combination of a resistor and a capacitor [36]. For each test solution, a blank experiment (without membrane) was carried out in order to measure the solution resistance; membrane resistance R_m is then calculated by subtracting solution resistance from overall resistance (R_{m+s}).

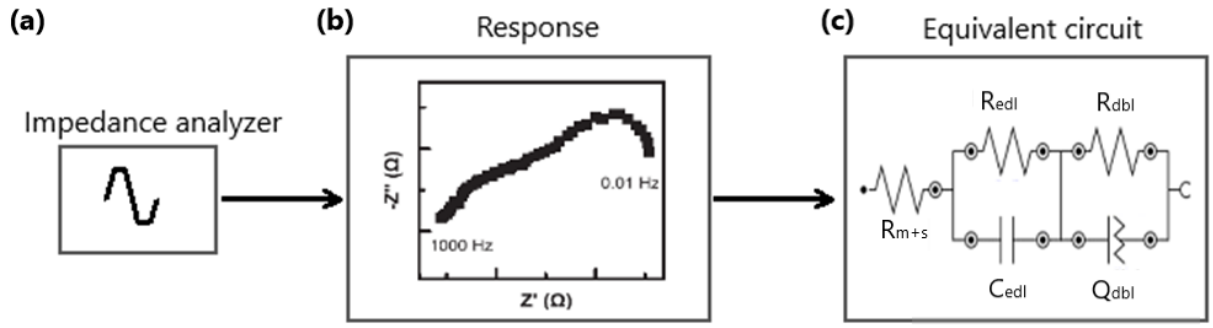

Figure 3. Summary of the EIS procedure: a) impedance analyzer, b) plot of real (Z' (Ω)) and imaginary part (Z" (Ω)) of impedance, c) illustration of equivalent circuit for membrane and solution resistance, electrical double layer resistance and diffusion boundary layer resistance.

3. Results and discussion

3.1. SGP-RE tests

Natural seawater and river water under investigation contain 44.6 and 0.3 g/L of total dissolved salts, respectively. The ionic content is higher with respect to standard values reported in literature (35 g/L and 0.13 g/L, respectively); however, this salinity variation is an expected situation in restricted basins (i.e. Mediterranean sea) [37].

Fig. 4 illustrates current-voltage and current density-power density curves for natural and artificial solution at constant temperature of 20°C and at different flow rates. The maximum SGP-RE performance was observed for synthetic NaCl solutions fed at flow rate 40 $L \cdot h^{-1}$: gross P_d reached a maximum of 1.14 $W \cdot m^{-2}$ at current density of 15 $A \cdot m^{-2}$, OCV attained 3.96 V, and R_{stack} was 14.8 Ω. On the other hand, the poorest performance was detected when mixing natural seawater and river water at flow rate 20 $L \cdot h^{-1}$: gross P_d value and current density fell down to 0.29 $W \cdot m^{-2}$ and 5 $A \cdot m^{-2}$, respectively, while OCV decreased to 3.17 V and R_{stack} increased to 34.9 Ω. Use of natural solutions instead of synthetic ones resulted in a reduction of power density higher than 50%; this effect became more visible at higher flow rates. Eq. 5 illustrates the dependence of power density on OCV and R_{stack}. Although OCV is more influential on power density (squared

dependence), in our case the dominant decreasing parameter was R_{stack}; in fact, OCV values varied within a quite narrow range (3.1 – 4.0 V), while R_{stack} reduced significantly (from 35 to 14 Ω).

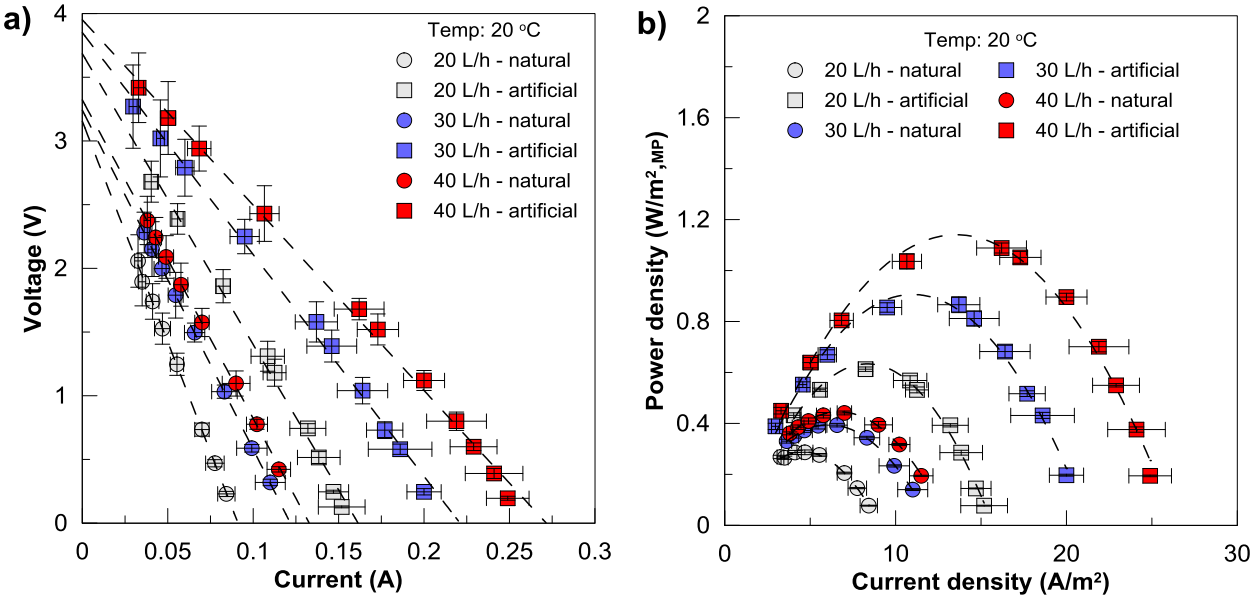

Figure 4. SGP-RE performance at 20°C and different flowrate: a) Voltage versus current; b) Gross power density versus current density.

Average permselectivity α_{ave} of Fuji-AEM-80045 and Fuji-CEM-80050 membranes can be calculated from Planck Henderson equation [5]:

$$E_{OCV} = 2N\frac{RT}{F}\frac{\alpha_{ave}}{z}\ln\left(\frac{a_s}{a_r}\right) \quad (6)$$

where N is number of membranes, R is the universal gas constant (J $mol^{-1}\cdot K^{-1}$), T is the absolute temperature (K), F is the Faraday constant ($C\cdot mol^{-1}$), a_s is the activity of seawater solution ($mol\cdot l^{-1}$), a_r is the activity of river water solution ($mol\cdot l^{-1}$), and z is the ion valence (-). Activity coefficients were evaluated by PHREEQC v. 2.18.00 software [38].

Average permselectivity of the Fuji-AEM and CEM in artificial seawater and river water mixing was 68%, assuming a linear variation of solute concentration along the stack. As a comparison, Fontananova *et al.* (2017) reported permselectivity of Fuji-CEM and Fuji-AEM measured by *ex-situ* method as 96% and 93% (average: 94.5%), respectively, in 0.1//0.5 M pure NaCl solutions [39]. The lower permselectivity can be explained by the higher concentration gradient of feed solutions (from table 1, equivalent ionic strength is 0.012 and 0.958 molal for river water and seawater, respectively, for an HCC/LCC ratio of ~ 80) that enhances the co-ion transport against the chemical potential gradient [39,40]. Accordingly, for 0.1//5.0 M NaCl solutions (HCC/LCC ratio of ~ 50), Fontananova *et al.* (2017) observed a decrease of Fuji-CEM and Fuji-AEM permselectivity to 89% and 73%, respectively [39].

Table 3 summarizes the experimental data for OCV, resistance and P_d. In general, a step increase in flowrate from 20 to 30 $L \cdot h^{-1}$ improved P_d and decreased stack resistance more than a further increment from 30 to 40 $L \cdot h^{-1}$. For natural solutions, in the first case P_d enhanced by 38% while R_{stack} decreased by 23% whereas, in the second step, P_d enhanced by 10% while R_{stack} decreased only by 7%. Likewise, when flowrate of artificial solution was increased from 20 $L \cdot h^{-1}$ to 30 $L \cdot h^{-1}$, P_d increased by 48% and R_{stack} decreased by 24%; these values were limited to 27% and 16% in the case of flowrate enhancement from 30 to 40 $L \cdot h^{-1}$. Vermaas *et al.* (2011) observed that the diffusive boundary layer near the membranes induces a considerable resistance at lower flow rates [7]. Enhancing the non-ohmic resistances by improving fluid-dynamics (higher Reynolds number) is possible up to a certain extent; further increase in flow rate does not promote a significant gain in terms of gross P_d due to increase in pumping energy [41].

An additional reason for increasing power density at higher flow rates is related to the residence time of solutions within the stack. Higher residence time (at lower flowrate) results in a more

significant dilution of the HCC solution accompanied by a more significant concentration of the LCC solution; the consequent decrease of concentration gradient across IEMs causes the decline of SGP-RE performance.

Table 3. Measured data from SGP-RE tests

		Natural Solutions			Artificial Solutions		
Flow rate L/h	**Temp. °C**	**OCV V**	**R_{stack} Ω**	**P_d W/m²**	**OCV V**	**R_{stack} Ω**	**P_d W/m²**
20	60	3.68	30.5	0.46	4.09	12.8	1.41
	40	3.54	33.2	0.39	4.10	14.5	1.26
	20	3.17	34.9	0.29	3.69	23.1	0.61
	10	3.02	37.7	0.24	3.48	32.4	0.38
30	20	3.25	26.8	0.40	3.86	17.6	0.90
40	20	3.32	25.0	0.44	3.96	14.8	1.14

In natural seawater, more than 10%w of cations were divalent ions (Mg^{2+} and Ca^{+}) and approximately 10%w of anions were divalent SO_4^{2-}. The evidence of the negative impact of divalent ions on the SGP-RE performance, is reported in literature [10,29,31,32,42]; hereafter we show that this effect - intrinsically associated to the ion valence z>1 in equation 6 – is mainly enforced by the increase in IEM resistance and the occurrence of Mg^{2+} and SO_4^{2-} transport against its concentration gradient.

Membrane resistance and permselectivity are significantly affected by the electrical interactions between bi-valent ions and fixed charged groups of IEMs; in particular, an increase in CEM resistance occurs due to crosslinking of two fixed anionic groups when bridged by Mg^{2+}; similarly, SO_4^{2-} ions cause an increase of AEM resistance by attracting each one a pair of fixed cationic

groups. Neutralization of some fixed groups reduces the effective charge density of IEMs; consequently, ineffective Donnan exclusion results in a low permselectivity [43]. Ion permselectivity depends on several factors, such as affinity of a specific ion to a given fixed group on the membrane and mobility of ions. The selectivity order of anions were stated by Sata (2000) [44] as:

$$I^- > NO_3^- \sim Br^- > NO_2^- > Cl^- > OH^- > SO_4^{2-} > F^-$$

while selectivity order for cations were reported by Strathmann (2004) [45] as:

$$Ba^{2+} > Sr^{2+} > Ca^{2+} > Mg^{2+} > H^+ > (Cu^{2+} \sim Zn^{2+} \sim Ni^{2+}) > K^+ > Na^+ > Li^+ > Fe^{3+}$$

According to permselectivity studies, it can be concluded Cl^- is preferred against SO_4^{2-} by AEM whereas Ca^{2+} and Mg^{2+} are preferred against Na^+ by CEM. Coherently, Avci *et al.* (2016) observed that CEM resistance is critically affected by Mg^{2+} concentration.

Fig. 5 shows the results from electrical tests on SGP-RE stack at different temperatures (10, 20, 40 and 60°C) for both natural and artificial seawater and river water. Under the same experimental conditions, mixing artificial NaCl solutions resulted in higher P_d and OCV, and lower R_{stack} than natural solutions. Presence of approximately 10%w multivalent ions reduced OCV due to the screening effect of fixed charge groups on IEMs as discussed before. However, for both natural and artificial solutions, the performance of SGP-RE unit increased with temperature due to higher transport rate of ions. Diffusion coefficients of Na^+ and Cl^- in 0.5 M NaCl were measured for Fuji-CEM-80050 and Fuji-AEM-80045, respectively, at different temperatures by Fontananova *et al.* (2014): a 24% and 80% increase were recorded for chloride and sodium ions, respectively, when increasing temperature from 20 to 40 ℃ [36]. At 60 °C, the maximum power density and OCV were 1.41 $W \cdot m^{-2}$ and 4.09 V, respectively, recorded for artificial feeds and R_{stack} reached its lowest value of 12.8 Ω. On the other hand, power density and OCV of natural feeds had a minimum at

0.24 $W \cdot m^{-2}$ and 3.02 V, respectively, when the experimental conditions designed considering winter conditions at 10 ℃.

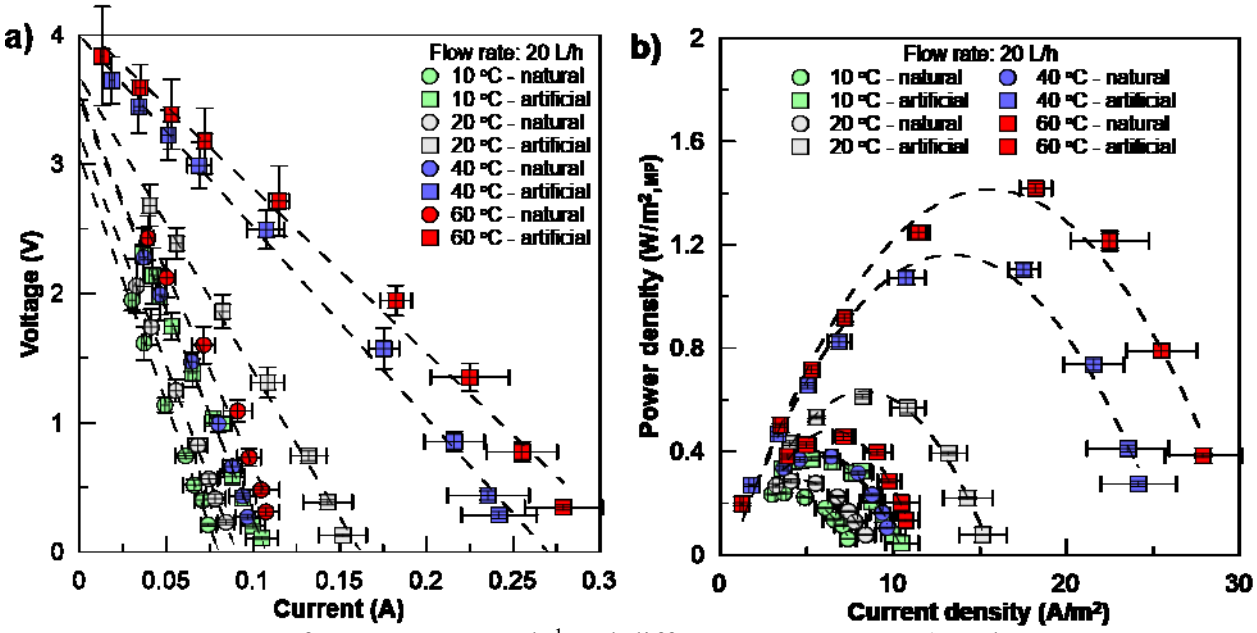

Figure 5. SGP-RE performance at 20 $L \cdot h^{-1}$ and different temperature: a) Voltage versus current; b) Gross power density versus current density.

Up to this point, the reported RED performance data were collected under steady-state conditions. Fig. 6 illustrates dynamic open circuit voltage response when a step change (10 L/h) applied to flow rate at 20 ℃. The OCV response of the lab scale RED stack were observed 20 min after the step change. Results show that reaching a new steady state OCV value takes 0.75-1.50 minutes which is 3-5 times of the residence time for both artificial and natural solutions mixing.

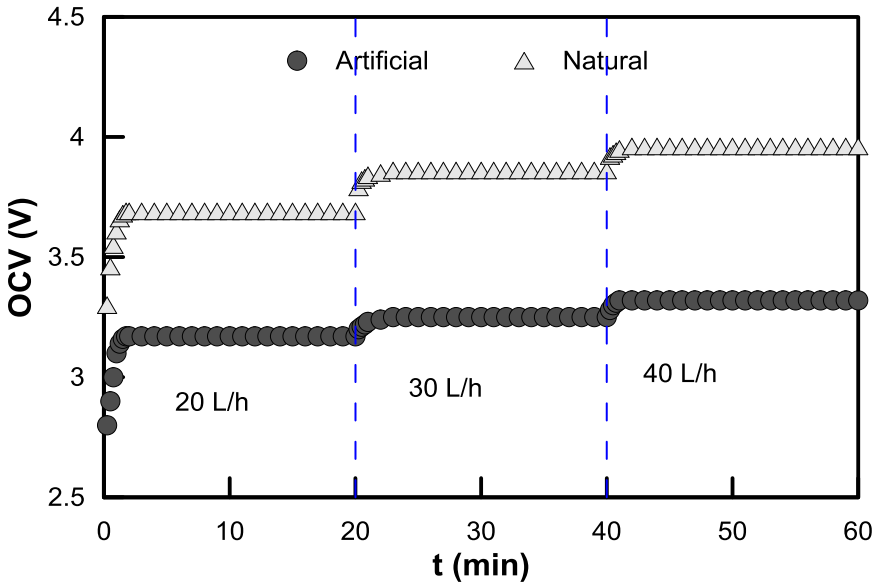

Figure 6. Dynamic response of OCV at 20 ℃

3.2. Uphill transport

Characterization of ion concentration in the inlet and outlet streams is essential for a deep understanding of mixing process and transport phenomena taking place within the SGP-RE unit. This investigation is important from both chemical and physical point of view, since different ions exhibit a different level of interactions with fixed charge groups located on IEMs. Figure 7 illustrates the influence of flowrate on ion transport at constant temperature (20°C). As expected, increasing flowrate ended up with a decreased number of transported ions for major monovalent species (Cl^- and Na^+) for both artificial and natural solutions due to lower residence time. K^+, a minor monovalent ion, also contributed to the total flux by transporting in the same direction of concentration gradient. On the other hand, multi-valent ions like Mg^{2+}, Ca^{2+} and SO_4^{2-} showed transport along the opposite direction of concentration gradient; this phenomenon is known as "uphill transport" [29,31,32,42].

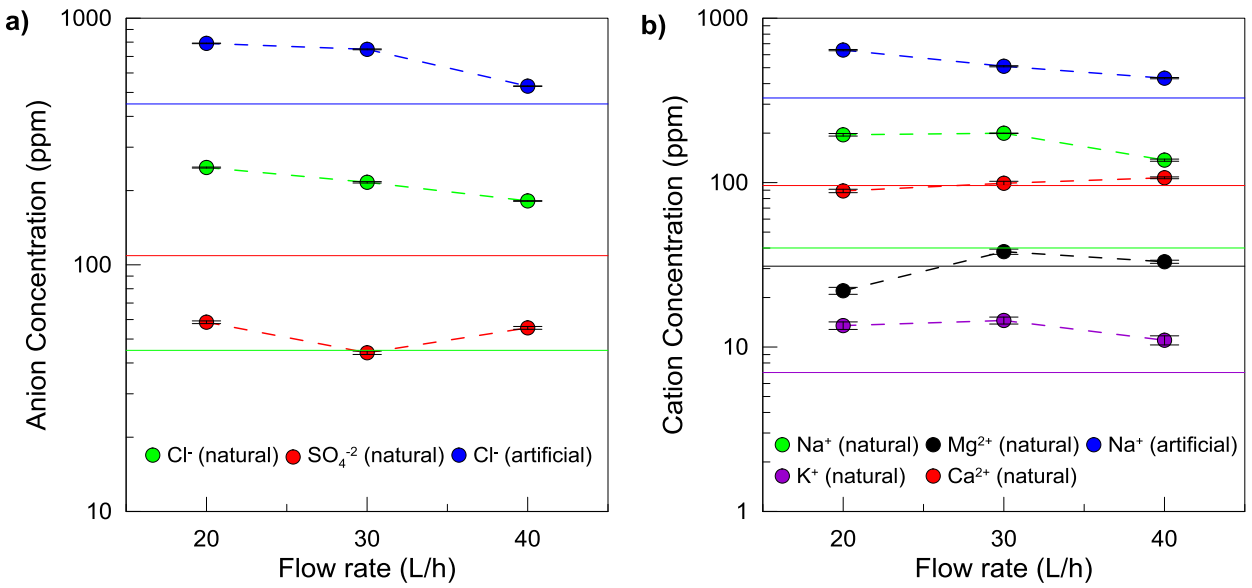

Figure 7. Transport of ions in LCC as a function of flowrate (temperature: 20°C): a) anions Cl^-, SO_4^{2-}; b) cations Na^+, K^+, Ca^{2+} and Mg^{2+}. Solid line with the same color of the symbol represents the inlet concentration of the corresponding ion, symbols are the outlet concentration of ions. Uphill transport occurs when symbols are below the corresponding solid lines.

Inter-diffusion between monovalent and multivalent ions occurs in other systems such as Donnan dialysis, driven by Donnan potential established between the membrane and the adjacent solution to maintain electroneutrality [31,32,42]. In SGP-RE, some previous studies carried out with artificial seawater and river water containing divalent ions, e.g. Mg^{2+} and SO_4^{2-}, reported the occurrence of uphill transport. Rijnaarts *et al.* (2017) theoretically explained the uphill transport over an ideal CEM exposed to 0.5 and 0.017 M saline solutions with 10% mol Mg^{2+}; cations start moving across the ion selective membrane under Donnan potential (0.079 V for Na^+ and 0.039 V for Mg^{2+}), until achieving Donnan equilibrium and maintaining charge neutrality (two Na^+ exchange for one Mg^{2+}) [42]. Investigations of Avci *et al.* (2016) provided evidence of uphill transfer in SGP-RE operated with NaCl-$MgCl_2$ solutions in the range of 0-30% of Mg^{2+} [29]. Fig. 8 shows the transported ions in LCC at temperatures of 20, 40 and 60°C with feed flowrate kept constant at 20 $L \cdot h^{-1}$. At increasing temperature, major monovalent ions exhibit a faster transport

along the concentration gradient, while multivalent ions Ca^{2+}, Mg^{2+} and SO_4^{2-} resulted in uphill transport at increasing mobility.

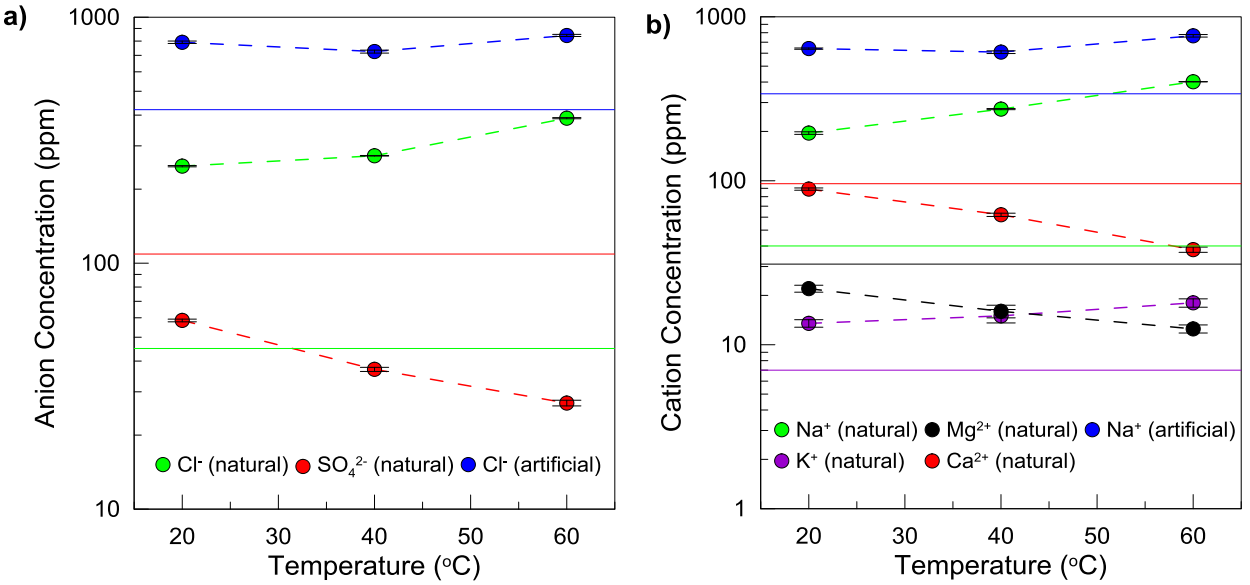

Figure 8. a) Transport of ions in LCC as a function of temperature (flowrate: 20 $L \cdot h^{-1}$): a) anions Cl^-, SO_4^{2-}; b) cations Na^+, K^+, Ca^{2+} and Mg^{2+}. Solid line with the same color of the symbol represents the inlet concentration of the corresponding ion, symbols are the outlet concentration of ions. Uphill transport occurs when symbols are below the corresponding solid lines.

3.3. Electrochemical Impedance Spectroscopy

Characterization of electrical properties of IEMs and their interfaces was done by Electrochemical Impedance Spectroscopy (EIS) [46]. In this study, a range of frequency from 0.01 to 1000 Hz was applied to analyze impedance of the membranes and electrolytes. In such a system, the total resistance is dectermined by ohmic resistances (i.e. membrane and solution resistances) and non-ohmic resistances (i.e. electrical double layer and diffusion boundary layer resistances) as it is shown by the electrical circuit (Fig. 3).

Charged groups fixed on the membrane surface attract the oppositely charged ions via Coulomb forces and create electrical double layer at the solid-liquid interface. Electrical double layer is composed of Stern layer and diffuse layer; strongly bounded ions - due to electrostatic interactions next to the membrane - form the Stern layer, while diffuse layer is caused by weak electrostatic interactions on the outer shell of electrical double layer [36].

Diffusion boundary layer arises from the difference between transport number of the membrane and the bulk solution. In an ideal IEM, electrical current is transported by counter ions because of the Donnan exclusion. On the other hand, in the bulk solution, univalent ions carry almost the same electrical current, and as a result, excluded ions get polarized as an additional layer [36].

In this work, EIS allowed the quantitative characterization of the different electrical resistances present in the system. Fig. 9 illustrates the impedance characterization of AEM-80045 and CEM-80050 membranes in natural feed streams. As expected, total membrane resistances were an order of magnitude higher when natural river water used. In particular, CEM offers 5-6 times higher resistance than AEM in both seawater and river water, confirming the high impact of divalent cations. The aforementioned charge screening effect by divalent ions cause neutralization of fixed charge groups and, ultimately, increase of membrane resistance. It is worth mentioning that, for all cases, the extent of non-ohmic resistances was negligible with respect to total resistance.

The increase in the stack resistance when feed streams were shifted from artificial to natural solutions can be therefore attributed prevalently to the increase in CEM resistance. When comparing the values of membrane resistance with respect to measurements in standard solutions presented in Table 2, no significant change was observed for AEM, while CEM resistance increased 5 times in natural seawater. A possible explanation is that the affinity of fixed charged

groups of a CEM to Na^+ is lower than that of multivalent ions such as Mg^{2+} and Ca^{2+} whereas, for AEM, the affinity to Cl^- is higher than that of SO_4^{2-}, thus determining a limited screening effect.

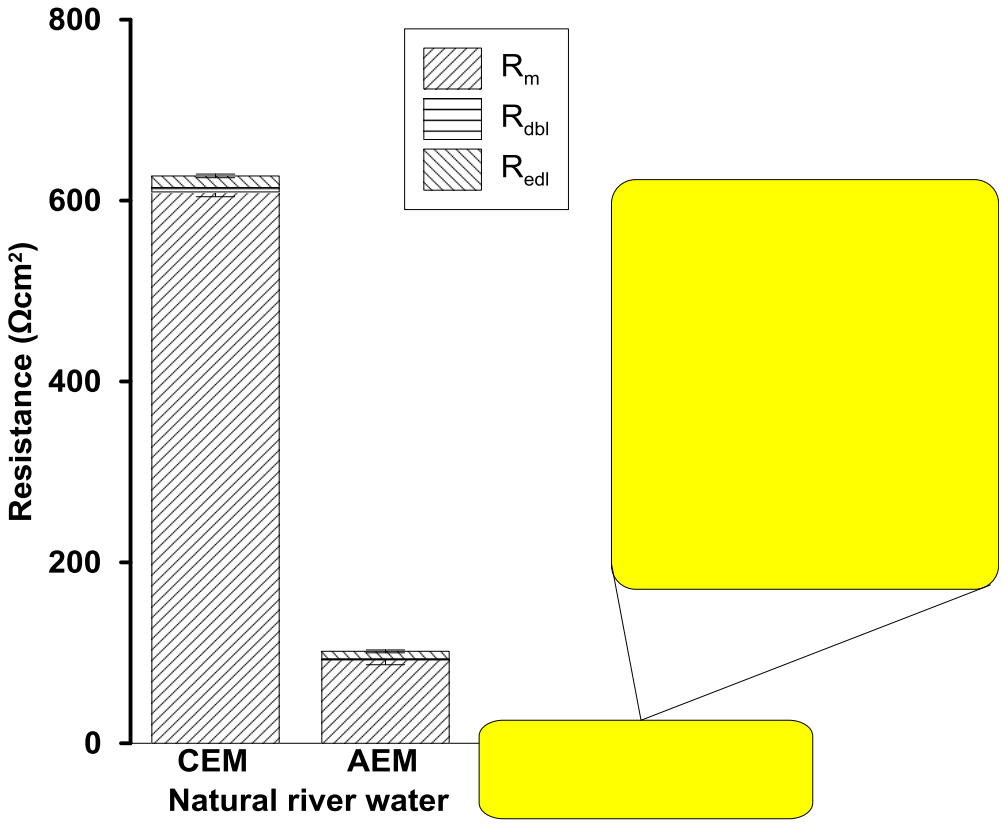

Figure 9. EIS of AEM-80045 and CEM-80050 in natural river water and seawater (R_m: membrane resistance; R_{dbl}: diffusive boundary layer resistance; R_{edl}: electrical double layer resistance).

The high resistance of IEMs in natural river water is coherent with the studies of Galama *et al.* (2014), who noted that membrane resistance mostly depends on the lowest external solution ion concentration and, below 0.3 M, it is limited by the conductivity of ionic solution [47].

Concerning the non-ohmic resistances, electrical double layer and diffusion boundary layer resistances were, respectively, one and two order of magnitude lower than ohmic resistances, for both AEM and CEM. Non-ohmic resistances in river water were about 10 times lower than those

measured in seawater. For natural seawater, non-ohmic resistances on CEM were higher than on AEM because of the higher different mobility of chloride with respect to sodium (u_{Cl-}/u_{Na+} = 1.5 [48]). Dlugulecki *et al.* (2010) observed that non-ohmic resistances are affected by the hydrodynamics of the system; on the other hand, ohmic resistances depend on temperature [48]. The values of total stack resistance reported in Table 3 agree with these assumptions: increasing flowrate from 20 to 40 $L \cdot h^{-1}$ resulted in 42% and 36% reduction in R_{stack} for natural and artificial solutions, respectively. Moreover, raising the temperature from 20 °C to 60 °C led to 13% and 44% reduction of R_{stack} for natural and artificial solutions, respectively.

In Fig. 10, the Nyquist plot of Fuji-AEM-80045 and Fuji-CEM-80050 at natural sea (Fig. 10 – a) and river water (Fig. 10 – b) conditions demonstrates the real and imaginary parts of the impedance. R_{m+s} can be distinguished easily at high frequency, i.e. 1000 Hz. Non-ohmic resistances, R_{edl} and R_{dbl}, can also be calculated by fitting the equivalent circuit in Fig. 3 – c. The Nyquist response of CEM shifted to the higher values compared to AEM confirms that the ohmic resistance of the CEM is higher than the AEM's. Similarly, enlarged amplitude of the Nyquist curves indicates an increase in the non-ohmic resistance, e.g: enlargement from AEM to CEM and enlargement from seawater to river water.

Figure 10. Nyquist plot of the Fuji-AEM-80045 and Fuji-CEM-80050 at 20 °C in a) natural seawater and b) natural river water

4. Conclusion

Tests with the natural solutions provide reliable data on the realistic potential and current limitation of RE. In this study, energy generation by SGP-RE from natural seawater/river water solutions and equivalent (in terms of ionic strength) NaCl solutions were investigated at different temperatures and flow rates. All artificial solutions resulted in higher power density, higher OCV and lower R_{stack}. At best, 1.41 $W \cdot m^{-2}$ maximum gross power density was extracted when operating with artificial NaCl solutions at 60 ºC, with highest recorded OCV (3.68 V) and lowest R_{stack} (30.5 Ω). On the other hand, SGP-RE performance with natural feeds was significantly reduced as a result of increased IEM resistance, reduced OCV and occurrence of uphill transport for Ca^{2+}, Mg^{2+} and SO_4^{2-}. In principle, the presence of uphill transport mainly leads to a reduction in OCV and the change in OCV when switching from artificial to the natural solution was about 19 % whereas the stack resistance increased by about 34 %. This indicates that the reduction in power density was mainly attributed to the change in stack resistance with CEMs playing a major role. The area resistance for CEM in natural seawater was significantly high reaching up to 10.6 Ωcm^2 which was about 3.5 times that of the area resistance in artificial feed solutions (3.0 Ωcm^2). This also marks an observable difference from the membrane resistance traditionally measured in 0.5 M NaCl solutions which, for instance, varies in the range of 0.9 – 3.1 Ωcm^2 for homogeneous CEMs [49]. Thus, the observed trend of membrane resistances under realistic natural solutions reported in the present study help in further elucidation of the behavior of IEMs, design and clarification of techno-economic requirement for practical application of RED.

Overall, results revealed the necessity to implement appropriate pretreatment to soften the feed solutions; additionally, further advances on membrane materials and manufacturing strategies are

needed in order to enhance both the efficiency of monovalent ions transfer and the rejection of multivalent ions.

Acknowledgments

The financial support of the Education, Audiovisual and Culture Executive Agency (EACEA-EU) within the programme EUDIME "Erasmus Mundus Doctorate in Membrane Engineering" (FPA 2011–0014, SGA 2014–0970, http://eudime.unical.it) is kindly acknowledged. R. A. Tufa acknowledges the financial support of the European Union's Horizon 2020 research and innovation programme under the Marie Skłodowska-Curie Actions IF Grant agreement No. 748683.

References

[1] International Energy Outlook 2013, https://www.eia.gov/outlooks/ieo/pdf/0484(2013).pdf; 2013 (accessed in 22 February 2018)

[2] Pattle RE, Production of electric power by mixing fresh and salt water in the hydroelectric pile, Nature 1954;174:660.

[3] Ruud Kempener FN, Salinity gradient energy, http://eusew.eu/sites/default/files/energy_days/Sal%20Grad%20Background%20doc%20.pdf. 2014 (accessed in 22 February 2018)

[4] Daniilidis A, Vermaas DA, Herber R, Nijmeijer K, Experimentally obtainable energy from mixing river water, seawater or brines with reverse electrodialysis, Renew. Energy. 2014;64:123–31.

[5] Weinstein JN, Leitz FB, Electric Power from Differences in Salinity: The Dialytic Battery, Science 1976;191:557–9.

[6] Veerman J, Saakes M, Metz SJ, Harmsen GJ, Reverse electrodialysis: Performance of a stack with 50 cells on the mixing of sea and river water, J. Memb. Sci. 2009;327:136–44.

[7] Vermaas DA, Saakes M, Nijmeijer K, Doubled power density from salinity gradients at reduced intermembrane distance., Environ. Sci. Technol. 2011;45:7089–95.

[8] Brauns E, An alternative hybrid concept combining seawater desalination, solar energy and reverse electrodialysis for a sustainable production of sweet water and electrical energy, Desalin. Water Treat. 2010;13:53–62.

[9] Tufa RA, Rugiero E, Chanda D, Hnàt J, van Baak W, Veerman J, Fontananova E, Di Profio G, Drioli E, Bouzek K, Curcio E, Salinity gradient power-reverse electrodialysis and alkaline polymer electrolyte water electrolysis for hydrogen production, J. Memb. Sci. 2016;514:155–64.

[10] Tufa RA, Curcio E, Van Baak W, Veerman J, Grasman S, Fontananova E, Di Profio G, Potential of brackish water and brine for energy generation by salinity gradient power-reverse electrodialysis (SGP-RE), RSC Adv. 2014;4:42617–23.

[11] Tufa RA, Curcio E, Brauns E, Van Baak W, Fontananova E, Di Profio G, Membrane Distillation and Reverse Electrodialysis for Near-Zero Liquid Discharge and low energy seawater desalination, J. Memb. Sci. 2015;496:325–33.

[12] Turek M, Bandura B, Dydo P, Power production from coal-mine brine utilizing reversed electrodialysis, Desalination. 1008;221:462–6.

[13] Tedesco M, Brauns E, Cipollina A, Micale G, Modica P, Russo G, Helsen J, Reverse Electrodialysis with saline waters and concentrated brines: a laboratory investigation towards technology scale-up, J. Memb. Sci. 2015;492:9–20.

[14] Tedesco M, Scalici C, Vaccari D, Cipollina A, Tamburini A, Micale G, Performance of the first Reverse Electrodialysis pilot plant for power production from saline waters and concentrated brines, J. Memb. Sci. 2016;500:33–45.

[15] Emdadi A, Gikas P, Farazaki M, Emami Y, Salinity gradient energy potential at the hyper saline Urmia Lake - Zarrineh Rud River system in Iran, Renew. Energy. 2016;86:154–62.

[16] Wick GL, Power from salinity gradients, Energy. 1978;3:95–100.

[17] Post JW, Veerman J, Hamelers HVM, Euverink GJW, Metz SJ, Nymeijer K, Buisman CJN, Salinity-gradient power: Evaluation of pressure-retarded osmosis and reverse electrodialysis, J. Memb. Sci. 2007;288:218–30.

[18] Veerman J, de Jong RM, Saakes M, Metz SJ, Harmsen GJ, Reverse electrodialysis: Comparison of six commercial membrane pairs on the thermodynamic efficiency and power density, J. Memb. Sci. 2009;343:7–15.

[19] Güler E, Elizen R, Saakes M, Nijmeijer K, Micro-structured membranes for electricity generation by reverse electrodialysis, J. Memb. Sci. 2014;458:136–48.

[20] Güler E, Elizen R, Vermaas DA, Saakes M, Nijmeijer K, Performance-determining membrane properties in reverse electrodialysis, J. Memb. Sci. 2013;446:266–76.

[21] Hong JG, Chen Y, Nanocomposite reverse electrodialysis (RED) ion-exchange membranes for salinity gradient power generation, J. Memb. Sci. 2014;460:139–47.

[22] Veerman J, Post JW, Saakes M, Metz SJ, Harmsen GJ, Reducing power losses caused by ionic shortcut currents in reverse electrodialysis stacks by a validated model, J. Memb. Sci. 20089;310:418–30.

[23] Vermaas DA, Saakes M, Nijmeijer K, Enhanced mixing in the diffusive boundary layer for energy generation in reverse electrodialysis, J. Memb. Sci. 2014;453:312–9.

[24] Długołęcki P, Dąbrowska J, Nijmeijer K, Wessling M, Ion conductive spacers for increased power generation in reverse electrodialysis, J. Memb. Sci. 2010;347:101–7.

[25] Veerman J, Saakes M, Metz SJ, Harmsen GJ, Electrical power from sea and river water by reverse electrodialysis: a first step from the laboratory to a real power plant, Environ. Sci. Technol. 2010;44:9207–12.

[26] Jagur-Grodzinski J, Kramer R, Novel process for direct conversion of free energy of mixing into electric power, Ind. Eng. Chem. Process Des. Dev. 1986;25:443–9.

[27] Suda F, Matsuo T, Ushioda D, Transient changes in the power output from the concentration difference cell (dialytic battery) between seawater and river water, Energy. 2007;32:165–73.

[28] Turek M, Bandura B, Renewable energy by reverse electrodialysis, Desalination. 2007;205:67–74.

[29] Avci AH, Sarkar P, Tufa RA, Messana D, Argurio P, Fontananova E, Di Profio G, Curcio E, Effect of Mg2+ ions on energy generation by Reverse Electrodialysis, J. Memb. Sci. 2016;520:499–506.

[30] Farrell E, Hassan MI, Tufa RA, Tuomiranta A, Avci AH , Politano A, Curcio E, Arafat HA, Reverse electrodialysis powered greenhouse concept for water- and energy-self-sufficient agriculture, Appl. Energy. 2017;187:390–409.

[31] Vermaas DA, Veerman J, Saakes M, Nijmeijer K, Influence of multivalent ions on renewable energy generation in reverse electrodialysis, Energy Environ. Sci. 2014;7:1434–45.

[32] Post JW, Hamelers HVM, Buisman CJN, Influence of multivalent ions on power production from mixing salt and fresh water with a reverse electrodialysis system, J. Memb. Sci. 2009;330: 65–72.

[33] Vermaas DA, Kunteng D, Saakes M, Nijmeijer K, Fouling in reverse electrodialysis under natural conditions., Water Res. 2013;47:1289–98.

[34] Pawlowski S, Galinha CF, Crespo JG, Velizarov S, Prediction of reverse electrodialysis performance by inclusion of 2D fluorescence spectroscopy data into multivariate statistical models, Sep. Purif. Technol. 2015;150:159–69.

[35] Pawlowski S, Galinha CF, Crespo JG, Velizarov S, 2D fluorescence spectroscopy for monitoring ion-exchange membrane based technologies - Reverse electrodialysis (RED), Water Res. 2016;88:184–98.

[36] Fontananova E, Zhang W, Nicotera I, Simari C, van Baak W, Di Profio G, Curcio E, Drioli E, Probing membrane and interface properties in concentrated electrolyte solutions, J. Memb. Sci. 2014;459:177–89.

[37] Kennish MJ, Practical Handbook of Marine Science, 3th ed., Boca Raton, FL: CRC Press LLC; 2001.

[38] Parkhurst DL, Appelo CAJ, User's Guide To PHREEQC (version 2) — a Computer Program for Speciation Batch-Reaction, One-Dimensional Transport, and Inverse Geochemical Calculations, Water-Resources Investig. Rep. 99-4259 1999

[39] Fontananova E, Messana D, Tufa RA, Nicotera I, Kosma V, Curcio E, Van Baak W, Drioli E, Di Profio G, Effect of solution concentration and composition on the electrochemical properties of ion exchange membranes for energy conversion, J. Power Sources. 2017;340:282–93.

[40] Zlotorowicz A, Strand RV, Burheim OS, Kjelstrup S, The permselectivity and water transference number of ion exchange membranes in reverse electrodialysis, J. Memb. Sci. 2017;523:402–8.

[41] Pawlowski S, Rijnaarts T, Saakes M, Nijmeijer K, Crespo JG, Improved fluid mixing and power density in reverse electrodialysis stacks with chevron-profiled membranes, J. Memb. Sci. 2017;531:111–21.

[42] Rijnaarts T, Huerta E, Van Baak W, Nijmeijer K, Effect of Divalent Cations on RED Performance and Cation Exchange Membrane Selection to Enhance Power Densities, Environ. Sci. Technol. 2017;51:13028–35.

[43] Geise GM, Paul DR, Freeman BD, Fundamental water and salt transport properties of polymeric materials, Prog. Polym. Sci. 2014;39:1–42.

[44] Sata T, Studies on anion exchange membranes having permselectivity for specific anions in electrodialysis - effect of hydrophilicity of anion exchange membranes on permselectivity of anions, J. Memb. Sci. 2000;167:1–31.

[45] Strathmann H, Ion-Exchange Membrane Separation Processes, Amsterdam, The Netherlands, Elsevier B.V, 2004.

[46] Barsoukov E, Macdonald JR, Impedance Spectroscopy Theory, Experiment, and Applications, 2nd ed. Hoboken, New Jersey, Wiley-Interscience, 2005.

[47] Galama AH, Vermaas DA, Veerman J, Saakes M, Rijnaarts HHM, Post JW, Nijmeijer K, Membrane resistance: The effect of salinity gradients over a cation exchange membrane, J. Memb. Sci. 2014;467:279–91.

[48] Długołęcki P, Ogonowski P, Metz SJ, Saakes M, Nijmeijer K, Wessling M, On the resistances of membrane, diffusion boundary layer and double layer in ion exchange membrane transport, J. Memb. Sci. 2010;349:369–79.

[49] Hong JG, Zhang B, Glabman S, Uzal U, Dou X, Zhang H, Wei X, Chen Y, Potential ion exchange membranes and system performance in reverse electrodialysis for power generation: A review, J. Memb. Sci. 2015;486:71–88.